

Marquette University

e-Publications@Marquette

Biological Sciences Faculty Research and
Publications

Biological Sciences, Department of

9-2011

Self-Assembly of *Escherichia coli* MutL and Its Complexes with DNA

Anita Niedziela-Majka

Washington University School of Medicine in St. Louis

Nasib K. Maluf

University of Colorado Denver

Edwin Antony

Marquette University, edwin.antony@marquette.edu

Timothy M. Lohman

Washington University School of Medicine in St. Louis

Follow this and additional works at: https://epublications.marquette.edu/bio_fac



Part of the [Biology Commons](#)

Recommended Citation

Niedziela-Majka, Anita; Maluf, Nasib K.; Antony, Edwin; and Lohman, Timothy M., "Self-Assembly of *Escherichia coli* MutL and Its Complexes with DNA" (2011). *Biological Sciences Faculty Research and Publications*. 417.

https://epublications.marquette.edu/bio_fac/417

Marquette University

e-Publications@Marquette

Biological Sciences Faculty Research and Publications/College of Arts and Sciences

This paper is NOT THE PUBLISHED VERSION; but the author's final, peer-reviewed manuscript. The published version may be accessed by following the link in the citation below.

Biochemistry, Vol. 50, No. 37 (September 20, 2011): 7868–7880. [DOI](#). This article is © American Chemical Society Publications and permission has been granted for this version to appear in [e-Publications@Marquette](#). American Chemical Society Publications does not grant permission for this article to be further copied/distributed or hosted elsewhere without the express permission from American Chemical Society Publications.

Self-Assembly of *Escherichia coli* MutL and Its Complexes with DNA

Anita Niedziela-Majka

Department of Biochemistry and Molecular Biophysics, Washington University School of Medicine, St. Louis, Missouri

Nasib K. Maluf

Department of Biochemistry and Molecular Biophysics, Washington University School of Medicine, St. Louis, Missouri

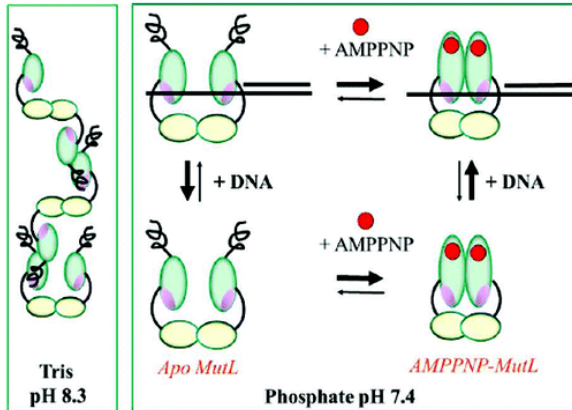
Edwin Antony

Department of Biochemistry and Molecular Biophysics, Washington University School of Medicine, St. Louis, Missouri

Timothy M. Lohman

Department of Biochemistry and Molecular Biophysics, Washington University School of Medicine, St. Louis, Missouri

Abstract



The *Escherichia coli* MutL protein regulates the activity of several enzymes, including MutS, MutH, and UvrD, during methyl-directed mismatch repair of DNA. We have investigated the self-association properties of MutL and its binding to DNA using analytical sedimentation velocity and equilibrium. Self-association of MutL is quite sensitive to solution conditions. At 25 °C in Tris at pH 8.3, MutL assembles into a heterogeneous mixture of large multimers. In the presence of potassium phosphate at pH 7.4, MutL forms primarily stable dimers, with the higher-order assembly states suppressed. The weight-average sedimentation coefficient of the MutL dimer in this buffer ($\bar{s}_{20,w}$) is equal to 5.20 ± 0.08 S, suggesting a highly asymmetric dimer ($f/f_0 = 1.58 \pm 0.02$). Upon binding the nonhydrolyzable ATP analogue, AMPPNP/ Mg^{2+} , the MutL dimer becomes more compact ($\bar{s}_{20,w} = 5.71 \pm 0.08$ S; $f/f_0 = 1.45 \pm 0.02$), probably reflecting reorganization of the N-terminal ATPase domains. A MutL dimer binds to an 18 bp duplex with a 3'-(dT₂₀) single-stranded flanking region, with apparent affinity in the micromolar range. AMPPNP binding to MutL increases its affinity for DNA by a factor of ~ 10 . These results indicate that the presence of phosphate minimizes further MutL oligomerization beyond a dimer and that differences in solution conditions likely explain apparent discrepancies in previous studies of MutL assembly.

FUNDING STATEMENT

This research was supported by National Institutes of Health Grant GM45948 to T.M.L.

In *Escherichia coli*, DNA replication errors are primarily corrected by the methyl-directed mismatch repair (MMR) pathway.(1) The MutL protein plays a central role in this process by regulating a number of events from mismatch recognition to DNA duplex unwinding.(2-4) MMR begins with recognition of the aberrant base pair by a MutS dimer in a process requiring ATP.(5) Subsequently, MutL, in an ATP-bound form, interacts with the MutS–DNA complex,(2, 6, 7) which activates a latent endonuclease associated with MutH. MutH then introduces a nick into the unmethylated (newly replicated) DNA strand at the nearest hemimethylated d(GATC) site, which can be positioned on either side of the mismatch.(8) The mechanistic details of this process are not fully understood, although models have proposed either looping of the intervening DNA or conversion of MutS into a sliding clamp that can then search for the nearest hemimethylated site.(9-12) In the next step, MutL recruits the UvrD protein, a 3' to 5' superfamily 1 (SF 1) DNA helicase,(13-15) to the nicked DNA substrate. In MMR, UvrD initiates DNA unwinding from the nick and proceeds past the mismatch, which can be as long as 1–2 kb in length.(16) The unwound nascent DNA strand is digested by cellular exonucleases,(17, 18) resulting in a gap that is then filled in by DNA polymerase III, with the final nick sealed by DNA ligase.(19)

The mechanism by which MutL stimulates the UvrD helicase, which by itself has a rather low unwinding processivity,(20) to unwind longer stretches of DNA is not fully understood.(21) It has been shown that MutL increases the unwinding activity of UvrD in vitro more than 1 order of magnitude under multiple-turnover conditions(22) and that the C-terminus of MutL interacts with the N- and C-termini of UvrD.(23)

MutL possesses a weak ATPase activity that is essential for MMR and is further stimulated ~5-fold by single-stranded DNA (ssDNA) binding.(6, 24, 25) Moreover, ATP binding by MutL, but not hydrolysis, is required to stimulate the activity of UvrD.(6) On the basis of these observations, a model was proposed in which MutL functions by continually loading multiple UvrD helicases onto a DNA substrate, thus facilitating unwinding of long stretches of DNA.(21, 26) It was also suggested that MutL loads UvrD onto the appropriate DNA strand to ensure that unwinding will proceed in the direction of the mismatch.(21, 26) This would prevent bidirectional DNA unwinding from the nick, as was observed in vitro in the absence of MutL.(15, 27)

UvrD self-associates into dimers and tetramers in vitro.(28) Furthermore, pre-steady state kinetic experiments demonstrated that the UvrD dimer possesses helicase activity.(29-33) Although a UvrD monomer is capable of translocating along ssDNA with 3' to 5' directionality and high processivity, a monomer does not unwind DNA processively in vitro.(34-36) Therefore, a plausible mechanism for explaining the stimulation of the helicase activity of UvrD by MutL could be that MutL stabilizes the UvrD dimer (or a higher-order oligomer). Alternatively, MutL may activate the helicase activity of the UvrD monomer. This could be accomplished by relieving the autoinhibition function of the 2B subdomain of UvrD. Such autoinhibitory activity of the 2B subdomain was unequivocally demonstrated for the Rep helicase.(37)

Crystal structures are available for both the N- and C-terminal regions of the *E. coli* MutL protein. The C-terminal 20 kDa region of MutL crystallizes as a dimer,(7) whereas the N-terminal 40 kDa ATPase domain of MutL crystallizes as a monomer in the absence of nucleotide; however, a dimer is observed in the presence of a nonhydrolyzable ATP analogue, with one AMPPNP bound per subunit. In this structure, part of the protein-protein interface and the lid of the ATP binding pocket are created upon folding of ~60 amino acid residues surrounding the nucleotide binding site.(24, 38)

On the basis of glycerol gradient centrifugation and gel filtration chromatography [at 3 °C in 50 mM potassium phosphate (pH 7.4), 50 mM KCl, 0.1 mM EDTA, and 1 mM DTT], MutL was reported to be an elongated dimer.(39) The dimensions of the MutL dimer calculated from light scattering experiments [at 24 °C in 20 mM Tris (pH 8.0), 200 mM KCl, 5 mM MgCl₂, 1 mM DTT, and 0.1 mM EDTA](7) differ substantially from the values obtained in the gel filtration experiments. Both sets of experiments were performed in different buffer and temperature conditions, and the effect of MutL concentration on the assembly state of MutL was not examined systematically.

MutL seems to be a very versatile macromolecule: it interacts with and regulates activities of many proteins participating in MMR.(1, 21) To decipher the molecular mechanism of this regulation and to understand how MutL stimulates UvrD helicase activity, it is necessary to understand the self-assembly properties of MutL and its interaction with DNA. Toward this end, we have examined the self-association properties of MutL over a range of solution conditions using both sedimentation equilibrium and velocity methods, as well as its interaction with an 18 bp DNA duplex possessing a 3'-dT₂₀ tail [3'(dT₂₀)-ds18].

Materials and Methods

Buffers

Buffers were made with reagent grade chemicals and distilled water that was further deionized by treatment with a Milli-Q water purification system (Millipore Corp., Bedford, MA). Spectrophotometric grade glycerol was from Aldrich (Milwaukee, WI). Buffer K consisted of 24.3 mM KH₂PO₄, 5.7 mM K₂HPO₄, 50 mM KCl, 2 mM 2-mercaptoethanol, and 0.2 mM PMSF (pH 7.4 at 25 °C). For the composition of all other buffers, see Table 1. Stock solutions of AMPPNP (5'-adenylylimidodiphosphate lithium) (Sigma-Aldrich, St. Louis, MO) were prepared in Milli-Q H₂O, neutralized to pH 7.5 by titration with NaOH, and stored in 10 µL aliquots at -20 °C. The AMPPNP

concentration was determined spectrophotometrically using an extinction coefficient of $15.4 \times 10^3 \text{ M}^{-1} \text{ cm}^{-1}$ at 259 nm.

Table 1. Compositions of Buffers

buffer	composition
TGN10/20/20	10 mM Tris (pH 8.3 at 25 °C), 20% (v/v) glycerol, 20 mM NaCl, 1 mM 2-mercaptoethanol
M	40.5 mM KH_2PO_4 , 9.5 mM K_2HPO_4 (pH 7.4 at 25 °C), 50 mM KCl, 0.1 mM EDTA, 1 mM 2-mercaptoethanol
M+Tris	10 mM Tris (with desired pH), 50 mM KCl, 0.1 mM EDTA, 1 mM 2-mercaptoethanol
M20/20	40.5 mM KH_2PO_4 , 9.5 mM K_2HPO_4 (pH 7.4, 25 °C), 20% (v/v) glycerol, 20 mM NaCl, 0.1 mM EDTA, 1 mM 2-mercaptoethanol
N20/20	40.5 mM NaH_2PO_4 , 9.5 mM Na_2HPO_4 (pH 7.4, 25 °C), 20% (v/v) glycerol, 20 mM NaCl, 0.1 mM EDTA, 1 mM 2-mercaptoethanol

MutL Expression and Purification

MutL was expressed and purified to greater than 98% homogeneity as described previously,(39) but with the following modifications. BL21(DE3)pLysS cells were freshly transformed with MutL expression plasmid L1-pET3a, kindly provided by P. Modrich (Duke University Medical Center, Durham, NC). Cells were grown at 37 °C in 4 L of LB broth(40) supplemented with 1% glucose (w/v), 4 µg/mL thymine, 10 µg/mL thiamine, 10 mM potassium phosphate (pH 7.4 at 25 °C), 100 µg/mL ampicillin, and 35 µg/mL chloramphenicol. MutL expression was induced at an OD_{600} of 1.0 with 1 mM IPTG for 3.5 h. All purification steps were performed at 4 °C. Cells (25 g) were resuspended in ice-cold buffer containing 50 mM potassium phosphate, 1 mM EDTA, 2 mM 2-mercaptoethanol, and 0.2 mM PMSF (pH 7.4 at 25 °C) using 7 mL of buffer/g of paste. The suspension was incubated on ice for 30 min to allow disruption of bacterial cell walls by lysozyme expressed by plasmid pLysS, followed by incubation for 30 min with 0.05% (w/v) sodium deoxycholate. The viscosity of the lysate was reduced by sonication on ice for 2–5 min using 15–30 s bursts at 50% duty and a power setting of 7 (model W225, Heat System-Ultrasonics, Inc., Farmingdale, NY). Streptomycin sulfate and ammonium sulfate precipitation was performed as described previously.(39) An ammonium sulfate pellet was dissolved in 200 mL of buffer K, and the resulting solution was clarified by centrifugation at 13000 rpm for 45 min and divided into two 100 mL pools that were purified sequentially on a ceramic hydroxyapatite column (CHT type I, Bio-Rad, Hercules, CA). The protein solution (100 mL) was loaded (10 mL/min) onto ceramic hydroxyapatite resin (50 mL) equilibrated with buffer K while being mixed with buffer K such that the conductivity was no higher than that of buffer K containing 75 mM potassium phosphate. Hydroxyapatite chromatography was performed as described previously.(39) Fractions containing MutL were pooled and loaded onto a Poros 50 HS strong cation exchange column (50 mL) (Applied Biosystems, Foster City, CA) equilibrated with buffer K. The column was loaded (10 mL/min) while the protein solution was being mixed with buffer containing 30 mM potassium phosphate, 2 mM 2-mercaptoethanol, and 0.2 mM PMSF (pH 7.4 at 25 °C) to reduce the KCl concentration to 75 mM. The column was washed with buffer K (200 mL) and eluted with a 500 mL linear gradient of KCl (50 to 400 mM) in 30 mM potassium phosphate, 2 mM 2-mercaptoethanol, and 0.2 mM PMSF (pH 7.4 at 25 °C). MutL elutes at 300–350 mM KCl. Fractions containing MutL were pooled and dialyzed overnight versus buffer K. After clarification by centrifugation at 13000 rpm for 45 min, the protein was loaded (2 mL/min) onto a ssDNA cellulose column (50 mL) equilibrated with buffer K and washed with buffer K (200 mL) and then buffer (300 mL) containing 30 mM potassium phosphate, 100 mM KCl, 2 mM 2-mercaptoethanol, and 0.2 mM PMSF (pH 7.4 at 25 °C). MutL was eluted with 30 mM potassium phosphate, 250 mM KCl, 2 mM 2-mercaptoethanol, and 0.2 mM PMSF (pH 7.4 at 25 °C), and

pooled fractions were dialyzed versus storage buffer (buffer M). MutL aliquots in buffer M were flash-frozen in liquid nitrogen and stored at $-80\text{ }^{\circ}\text{C}$ ($5\text{--}6\text{ }\mu\text{M}$ monomer).

Prior to being used in the experiments, MutL protein was thawed at $10\text{ }^{\circ}\text{C}$ in an ice/water bath, centrifuged at 14000 rpm for 15 min at $4\text{ }^{\circ}\text{C}$, and dialyzed extensively into the appropriate buffer at $4\text{ }^{\circ}\text{C}$. The extinction coefficient of the MutL monomer in buffer M20/20 ($\epsilon_{280} = 50172 \pm 1204\text{ M}^{-1}\text{ cm}^{-1}$) was determined experimentally as described previously.(41)

DNA

Oligodeoxynucleotides were synthesized using an ABI model 391 DNA synthesizer (Applied Biosystems) and purified as described previously.(42, 43) The DNA used in this study [$3'\text{ss}(\text{dT})_{20}\text{ds}18\text{-Cy}3$] consisted of an 18 bp duplex with a $3'\text{-(dT)}_{20}$ single-stranded tail labeled with a Cy3 fluorophore at the 5'-end of the strand with a $3'\text{-ssDNA}$ tail. The sequence of the strand without the $3'\text{-ssDNA}$ tail was $5'\text{-GCCTCGCTGCCGTCGCCA-}3'$. Oligodeoxynucleotides were dialyzed into 10 mM Tris-HCl (pH 8.3) and stored at $-20\text{ }^{\circ}\text{C}$, and the concentration was determined spectrophotometrically as described previously(44) using an extinction coefficients of $5000\text{ M}^{-1}\text{ cm}^{-1}$ for Cy3 at 260 nm and $150000\text{ M}^{-1}\text{ cm}^{-1}$ at 550 nm (Glenn Research, Sterling, VA). We created the duplex DNA by mixing a 1:1 molar ratio of the two strands in 10 mM Tris-HCl and 50 mM NaCl (pH 8.3 at $25\text{ }^{\circ}\text{C}$), heating the sample to $95\text{ }^{\circ}\text{C}$ for 5 min, and then cooling it to room temperature over a period of 2 h. Duplex formation was confirmed by native polyacrylamide gel electrophoresis on a 10% acrylamide gel. DNA was dialyzed versus the appropriate buffer using 8000 Da molecular mass cutoff dialysis tubing (Spectrum Medical Industries, Inc., Houston, TX). The concentration of $3'\text{ss}(\text{dT})_{20}\text{ds}18\text{-Cy}3$ in buffer M20/20 was determined spectrophotometrically using an ϵ_{550} of $126311 \pm 2114\text{ M}^{-1}\text{ cm}^{-1}$ at 550 nm ($\epsilon_{260} = 460563 \pm 9011\text{ M}^{-1}\text{ cm}^{-1}$, and $\epsilon_{280} = 277722 \pm 6953\text{ M}^{-1}\text{ cm}^{-1}$).(28)

Analytical Ultracentrifugation

Dialyzed protein and DNA samples were filtered ($0.22\text{ }\mu\text{m}$ centrifugal filter devices, Ultrafree-MC, Millipore Corp., Bedford, MA) by centrifugation at 6000 rpm for 5 min at $4\text{ }^{\circ}\text{C}$. Sedimentation equilibrium and velocity experiments were performed using a ProteomeLab XL-A analytical ultracentrifuge equipped with an An50Ti rotor (Beckman Coulter, Fullerton, CA) at 5 or $25\text{ }^{\circ}\text{C}$. Absorbance data for MutL in the absence of DNA and AMPPNP were collected by scanning the sample cells at wavelengths of either 230 or 280 nm depending on the MutL concentration. In experiments performed with AMPPNP, the nucleotide at the same final concentration was placed in the reference channel of the centerpiece. Experiments performed with $35\text{ }\mu\text{M}$ AMPPNP were conducted at 230 or 280 nm. The contributions from the absorbance of $35\text{ }\mu\text{M}$ AMPPNP at the highest MutL concentration used ($3.78\text{ }\mu\text{M}$ MutL monomer) were 27 and 7% at 280 and 230 nm, respectively. For experiments performed with increasing AMPPNP concentrations, the cells were scanned at 292 nm where the absorbance of the nucleotide cofactor is minimal. Experiments performed with Cy3-labeled DNA were scanned at 550 nm. There was no absorbance change accompanying binding of MutL to $3'\text{ss}(\text{dT})_{20}\text{ds}18\text{-Cy}3$ duplex DNA.(28)

For sedimentation equilibrium, samples ($120\text{ }\mu\text{L}$) were loaded into the three channels of an Epon charcoal-filled six-channel centerpiece with $122\text{ }\mu\text{L}$ of buffer in the reference chambers. Absorbance data were collected by scanning the sample cells at wavelength intervals of 0.001 cm in the step mode with seven averages per step. Each experiment was conducted at three or four rotor speeds, starting with the lowest and finishing with the highest rotor speed. At each speed, samples were sedimented until they reached equilibrium (defined as successive superimposable scans taken 2 h apart). Sedimentation equilibrium data were edited using REEDIT (J. Lary, National Analytical Ultracentrifugation Center, Storrs, CT) to extract the data between the sample meniscus and the bottom of the cell chamber. The resulting concentration profiles were fitted to a sum of exponential terms (eq 1) using a nonlinear least-squares (NLLS) routine

(1)

$$A_T = \sum_{i=1}^n \exp[\ln A_{0,i} + \sigma_i(r^2 - r_{\text{ref}}^2)/2] + b$$

where A_T is the total absorbance at radial position r , $A_{0,i}$ is the absorbance of component i at the reference position (r_{ref}), and b is the baseline offset. The reduced molecular mass of component i , $\sigma_i = [M_i(1 - \bar{v}_i\rho)\omega^2]/RT$, where M_i is the molecular mass, \bar{v}_i is the partial specific volume, ρ is the buffer density, ω is an angular velocity of the rotor, T is the absolute temperature, and R is the gas constant. ρ was calculated from buffer composition using Sedenterp.(45) The NLLS fitting program WinNonlin(46) was used for analysis of concentration profiles obtained for a system with a single species ($n = 1$ in eq 1), whereas data for a multicomponent system ($n > 1$ in eq 1) were fitted with Scientist (Micromath Scientific Software, St. Louis, MO). The global NLLS fit of the absorbance profiles to eq 1 returns M for each component. For MutL at 25 °C, $\bar{v} = 0.7414$ mL/g as calculated from the amino acid composition according to eq 2(47) as implemented in Sedenterp,(45) where n_i is the number of amino acids of type i .

(2)

$$\bar{v} = \left(\sum_{i=1}^n n_i M_i \bar{v}_i \right) / \left(\sum_{i=1}^n n_i M_i \right)$$

Partial specific volumes at temperature T were calculated from the relationship $\bar{v}_T = \bar{v}_{25} + 4.25E^{-4}(T - 25)$.(48) The partial specific volume for 3'ss(dT)₂₀ds18-Cy3 duplex DNA was obtained experimentally by conducting sedimentation equilibrium experiments at three different loading concentrations (1.2, 2, and 4 μM) and four rotor speeds (18000, 22000, 27000, and 33000 rpm) at 25 °C in buffer M20/20. Absorbance data were collected at 550 nm, and 12 concentration profiles were fitted globally by NLLS methods with WinNonlin(46) using a single-ideal species model ($n = 1$ in eq 1). From the best fit value of the reduced molecular mass, a \bar{v}_{DNA} value of 0.5871 ± 0.0178 mL/g at 25 °C was calculated, assuming a molar mass calculated from the DNA composition ($M_{\text{Cy3-DNA}} = 17594.79$ g/mol). The weight-average \bar{v} for the MutL₂-DNA complex ($\bar{v}_{\text{MutL}_2\text{-DNA}} = 0.7237 \pm 0.002$ mL/g) and MutL₂ bound to AMPPNP in the absence ($\bar{v}_{\text{MutL}_2\text{-AMPPNP}} = 0.7392$ mL/g) and presence of DNA ($\bar{v}_{\text{MutL}_2\text{-DNA-AMPPNP}_2} = 0.7219 \pm 0.002$ mL/g) at 25 °C were calculated from \bar{v} and molar masses of the individual components ($M_{\text{MutL}_2} = 135847.9$ g/mol; $M_{\text{AMPPNP}} = 506.2$ g/mol) according to eq 2(47) (using $\bar{v}_{\text{ATP}} = 0.4421$ mL/g). The buoyant molecular weight of the complex can be calculated from the molar mass and the weight-average partial specific volume of the complex, with the equation $M_b = M(1 - \bar{v}\rho)$.

In sedimentation velocity experiments, the sample (380 μL) and buffer (392 μL) were loaded into each sector of an Epon charcoal-filled two-sector centerpiece. Experiments were performed at 25 or 5 °C and 42000 rpm. Absorbance data were collected every 2.5 min by scanning at the selected wavelength (230, 280, 292, or 550 nm) at intervals of 0.003 cm with one average in a continuous scan mode. The continuous sedimentation coefficient distribution, $c(s)$, was calculated using SEDFIT.(49, 50) The molar mass of the macromolecule can be estimated from the best fit values of sedimentation (s) and diffusion (D) coefficients according to eq 3.(51)

(3)

$$M = sRT/[D(1 - \bar{v}\rho)]$$

Calculated s values were converted to $s_{20,w}$ using Sedenterp.(45) Buffer density and viscosity were calculated from buffer composition using the tabulated values in Sedenterp.(45) Weight-average sedimentation

coefficients ($\bar{s}_{20,w}$) were calculated by integration of the area under the $c(s)$ curves.(52) The frictional coefficient ratio (f/f_o), where f is the frictional coefficient of the macromolecule and f_o is the frictional coefficient of a hydrated sphere of equivalent mass, was calculated using eq 4

(4)

$$\frac{f}{f_o} = \left[\frac{M^2(1 - \bar{v}\rho)^3}{162\pi^2(s_{20,w})^3 \eta^3 N_A^2 (\bar{v} + \delta v_{H_2O}^0)} \right]^{1/3}$$

where η , ρ , and $v_{H_2O}^0$ are the viscosity, density, and partial specific volume of pure water at 20 °C, respectively, N_A is Avogadro's number, and δ is the macromolecule hydration in grams of water bound per gram of macromolecule.(53, 54) An estimated value of the degree of hydration for MutL equal to δ (0.2806 g of water bound/g of protein) was used, based on the amino acid sequence of MutL and the method of Kuntz(55) as implemented in Sedenterp and applying the correction of Lin et al.,(56) which takes into account the fact that only ~70% of the water molecules calculated by Kuntz's method seems to be associated with folded proteins. For 3'(dT₂₀)-ds18-Cy3 DNA, a δ value of 0.497 g of water bound/g of DNA was used. This value was calculated on the basis of the weight-average contribution of single-stranded and double-stranded regions in the DNA molecule and the following published values: $\delta_{dsDNA} = 0.55$ g of water bound/g of DNA, and $\delta_{ssDNA} = 0.40$ g of water bound/g of DNA.(57, 58) For a MutL dimer bound to 3'(dT₂₀)-ds18-Cy3 DNA, a δ value of 0.305 g of water bound/g of protein–DNA complex was calculated from the weight-average of hydration of the MutL dimer and hydration of the DNA molecule.

Analysis of AMPPNP and DNA Binding to MutL

For AMPPNP binding to a MutL dimer [total concentration of MutL dimer ($M_{2,T}$) of 1.75 μ M], the dependence of the weight-average sedimentation coefficient ($\bar{s}_{20,w}$) on total AMPPNP concentration ($[X_T]$) was analyzed assuming two identical and independent nucleotide binding sites per MutL dimer, returning a stepwise microscopic association constant (k). Data were fit to eq 5 using the Scientist program (Micromath Scientific Software)

(5)

$$\bar{s}_{20,w} = \frac{C \times 2k[X_f] + D}{1 + k[X_f]}$$

where C and D are the $\bar{s}_{20,w}$ values for fully saturated and AMPPNP free MutL dimer, respectively, and $[X_f]$ is the concentration of free AMPPNP, equal to $[X_T]/(1 + 2k[M_{2,f}] + 2k^2[M_{2,f}][X_f])$, where $[M_{2,f}]$ is the concentration of free MutL dimer, equal to $[M_T]/(1 + 2k[X_f] + k^2[X_f]^2)$.

For DNA binding experiments (total DNA concentration, $[D_T]$, of 1.4 μ M), the dependence of \bar{s}_{app} on total MutL dimer concentration ($[M_{2,T}]$) was analyzed using a 1:1 binding isotherm model to obtain an apparent association equilibrium constant $K (=1/K_d)$. Data were fit implicitly to eq 6 using the Scientist program (Micromath Scientific Software)

(6)

$$\bar{s}_{app} = \frac{AK[M_{2,f}] + B}{1 + K[M_{2,f}]}$$

where K is an apparent association constant, $[M_{2,f}]$ is the concentration of free MutL dimer, $[M_{2,f}] = [M_{2,T}]/(1 + K[D_f])$, $[D_f]$ is the concentration of free DNA, equal to $[D_T]/(1 + K[M_{2,f}])$, A is the sedimentation coefficient of the MutL–DNA complex, and B is the sedimentation coefficient of free DNA.

Results

Assembly State of MutL

One goal of these studies was to determine a set of solution conditions that will allow us to study both MutL and UvrD separately and together in the presence and absence of a suitable DNA substrate. Toward this end, we performed a series of sedimentation velocity experiments to evaluate the oligomeric state of MutL in a variety of buffers and at a variety of protein concentrations. In the absence of DTT or 2-mercaptoethanol, we observed that a substantial fraction of MutL became covalently cross-linked via disulfide bond formation as detected by sodium dodecyl sulfate–polyacrylamide gel electrophoresis (data not shown). This cross-linking can be reversed by treatment with DTT or 2-mercaptoethanol (at millimolar concentrations). For this reason, all further experiments were performed in the presence of 1 mM 2-mercaptoethanol. Previous experiments by our laboratory that characterized the self-association properties and helicase activity of UvrD were performed in a Tris buffer.(28, 29, 59) Therefore, we first investigated the self-association properties of MutL under these same solution conditions, but including 1 mM 2-mercaptoethanol [buffer TGN10/20/20 (Table 1)]. Under these conditions, MutL displays a very broad and nonsymmetrical $c(s)$ distribution (Figure 1). Analysis of the $c(s)$ distribution(49, 50) in buffer TGN10/20/20 suggests that MutL exists as a heterogeneous mixture of species with sedimentation coefficients ranging from ~ 4.5 S (<8% of all species) for the smallest species to 10–55 S for larger species (Figure 1A). Under these conditions, we estimate a weight-average sedimentation coefficient ($\bar{s}_{20,w}$) of 29.1 S at 2 μ M MutL (total monomer concentration). With increasing NaCl concentrations in the TGN buffer from 20 to 100 mM, $\bar{s}_{20,w}$ decreased to 17.8 S at the same protein concentration, with approximately 28% of the MutL having an $s_{20,w}$ of 4.5 S, indicating a reduction in the average size of the oligomeric species (Figure 1A).

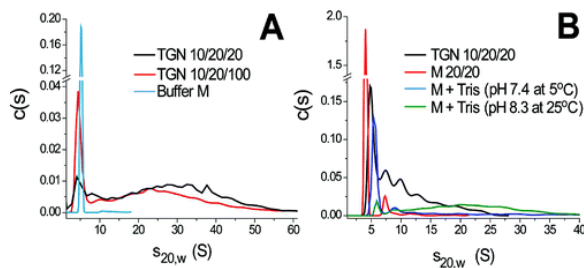


Figure 1. Continuous sedimentation coefficient distribution $c(s)$ analysis of MutL. MutL was dialyzed extensively into different buffers: TGN 10/20/20, TGN 10/20/100, buffer M, buffer M20/20, buffer M+Tris (Table1). Dialyzed protein was sedimented at 30,000 rpm at a loading concentration of 2 μ M monomer at 25 °C (A) or 3.2 μ M monomer at 5 °C (B). The absorbance scans were collected at 280 nm and analyzed using Sedfit, which approximate the mixture of macromolecular species as a system of noninteracting species with weight average frictional coefficient ratio $(f/f_o)_w$.

We next examined a buffer used by the Modrich laboratory (39) to study the MutL assembly state by sucrose gradient centrifugation and that we use to store our MutL preparations. This buffer (Buffer M, Table 1) contains 50 mM potassium phosphate (pH 7.4 at 25 °C), 50 mM KCl, 0.1 mM EDTA, 1 mM 2-mercaptoethanol. In Buffer M (25 °C), the $c(s)$ distribution displayed one major symmetrical peak with $s_{20,w} = 5.18 \pm 0.03$ S (Figure 1A), suggesting that MutL exists primarily as a single species (97% \pm 2%). Therefore, the solution conditions have a profound influence on the self-association properties of MutL. Buffer M contains potassium instead of sodium and phosphate instead of Tris and does not contain any glycerol. To assess the effect of individual buffer

constituents on the assembly state of MutL, we performed centrifugation experiments while systematically varying each component (Figure 1B and data not shown).

In the presence of 20% (v/v) glycerol and 20 mM NaCl in potassium phosphate buffer (buffer M20/20, Table 1), MutL displayed $c(s)$ distribution profiles similar to its behavior in Buffer M (see Figure 1B and Figure 5B for experiments at 5 and 25 °C, respectively). In buffer M20/20 at 5 °C, the $c(s)$ distribution shows a major symmetrical peak at $s_{20,w} \sim 4.5$ S (96% of total protein) and a minor peak at $s_{20,w} \sim 7.4$ S (3.5%), as well as minute quantities (0.06%) of some larger species suggesting that the glycerol and NaCl in buffer TGN 10/20/20 do not facilitate MutL aggregation (see below and Figure 5). Replacing potassium phosphate with sodium phosphate at pH 7.4 (buffer N20/20, Table 1) also does not affect the self-association properties of MutL ($\bar{s}_{20,w} = 4.60 \pm 0.02$ S, data not shown). Increasing the pH of buffer M from 7.4 to 8.3 also did not influence the sedimentation properties of MutL significantly ($\bar{s}_{20,w} = 4.79 \pm 0.02$ S, with $\sim 6\%$ of protein sedimented with higher $s_{20,w}$, data not shown). We also observed that lower temperatures reduced further aggregation of MutL, such that, even in Buffer TGN 10/20/20 at 5 °C around 32% of the protein sedimented with $s_{20,w} = 4.8$ S at a concentration of 3.2 μM monomer (buffer TGN 10/20/20, compare Figure 1B and Figure 1A). Substitution of potassium phosphate in buffer M with Tris (10 mM) (buffer M+Tris, Table 1) facilitated MutL self-assembly beyond the ~ 4.5 S species (Figure 1B). For example, in buffer M+Tris at pH 8.3 (value of pH at 25 °C) 94% of MutL sedimented with $s_{20,w}$ from 7.5 S – 45 S ($\bar{s}_{20,w} = 16.5$ S), whereas at pH 7.4 (value of pH at 5 °C) around 62% of MutL sedimented at $s_{20,w} = 5.6$ S with the rest of the protein sedimenting as a distribution of larger species (~ 9 to 50 S), with $\bar{s}_{20,w} = 9.4$ S (Figure 1B).

These experiments suggest that it is primarily the presence of PO_4^{3-} in buffer M that shifts the distribution of MutL oligomeric species to favor the smaller species. To estimate the molecular weight of this smallest MutL species, we analyzed the sedimentation velocity experiments by NLLS methods using SEDFIT (see Materials and Methods).⁽⁴⁹⁾ From the best fit values of sedimentation and diffusion coefficients, the molecular weight can be estimated using the Svedberg equation (eq 3 in Materials and Methods). The absorbance profiles were analyzed according to a two-species model, to account for a small amount (up to 3%) of a higher-order oligomeric species present in the MutL population, returning an M_{app} of 112 ± 5 kDa for the major species, suggesting a dimeric form of MutL (predicted molar mass of the MutL dimer equal to 135.8 kDa). Additional experiments showed no dependence of $\bar{s}_{20,w}$ on MutL concentration (Figure 2A), indicating that over the range studied (0.25–4 μM monomer) MutL exists as a single species, with an $\bar{s}_{20,w}$ of 5.20 ± 0.08 S. On the basis of this value, we estimate a frictional coefficient ratio, f/f_0 , of 1.58 ± 0.02 using eq 4 (Materials and Methods), where f/f_0 is the ratio of the frictional coefficient of the macromolecule to the frictional coefficient of a hydrated sphere with an identical molecular mass. This suggests that the MutL dimer is highly asymmetric under these solution conditions.

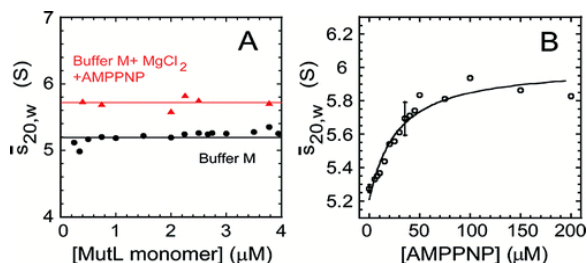


Figure 2. Weight-average sedimentation coefficient, $\bar{s}_{20,w}$, of MutL as a function of protein concentration (A) or AMPPNP concentration included in the buffer (B). Sedimentation velocity experiments were performed at 25 °C at different MutL concentrations (0.25–3.94 μM monomer loading concentrations) in buffer M (●) or buffer M with 1 mM MgCl_2 and 35 μM AMPPNP (▲) (A) or at a 1.75 μM MutL dimer loading concentration in buffer M with 1 mM MgCl_2 and different AMPPNP concentrations (B). The absorbance scans were collected at 280 or 230 nm (A) and at 292 nm (B) and analyzed using SEDFIT to obtain $c(s)$ distributions, which were integrated yielding $\bar{s}_{20,w}$. The smooth curve in panel B is a simulation using the best fit parameters derived from NLLS

analysis of the isotherm to a model assuming two identical and independent binding sites for AMPPNP on a single MutL dimer (eq 5 in Materials and Methods).

MutL possesses a weak ATPase activity that is stimulated several-fold by ssDNA.(24) It has been suggested that the binding of AMPPNP, a nonhydrolyzable ATP analogue, would induce a partial folding and dimerization of the N-terminus of MutL.(38) We therefore examined the effect of AMPPNP on the self-association properties of MutL using sedimentation velocity. MutL was dialyzed into buffer M, containing 1 mM MgCl₂, and then equilibrated with AMPPNP (35 μM) for 1 h at 25 °C before centrifugation. The addition of AMPPNP increased $\bar{s}_{20,w}$ from 5.20 ± 0.08 to 5.71 ± 0.08 S, in a manner independent of MutL concentration (Figure 2A). Using SEDFIT, a molecular mass of 112 ± 6 kDa was calculated for MutL, which is identical (within our uncertainty) to the value estimated in the absence of AMPPNP and MgCl₂. Experiments performed in buffer M with 1 mM MgCl₂ yielded an $\bar{s}_{20,w}$ that was similar to the value determined in the absence of AMPPNP and MgCl₂. Therefore, the increase in $s_{20,w}$ is solely due to AMPPNP binding to MutL (Figure 2B and data not shown). These results suggest that AMPPNP binding does not affect the oligomeric state of MutL, but rather its hydrodynamic shape such that the dimer becomes more compact, with an f/f_0 of 1.45 ± 0.02 .

To estimate the apparent affinity of AMPPNP for the MutL dimer, we performed a series of sedimentation velocity experiments at a constant MutL protein concentration (1.75 μM dimer loading concentration) as a function of AMPPNP concentration (buffer M with 1 mM MgCl₂). Figure 2B shows that $\bar{s}_{20,w}$ increases with AMPPNP concentration. NLLS analysis of the data using a model that assumes two identical and independent AMPPNP binding sites per MutL dimer (eq 5 in Materials and Methods) yields a binding constant of $(3.9 \pm 1.1) \times 10^4$ M⁻¹.

To further test whether the predominant assembly state of MutL is a dimer in its apo and AMPPNP/Mg²⁺-bound form, we performed sedimentation equilibrium studies in buffer M (Figure 3). Experiments were conducted at 5 °C to suppress aggregation of MutL beyond the smallest oligomeric state during the extended time of these experiments. Data were obtained at four rotor speeds (12000, 15000, 19000, and 23000 rpm) and several MutL loading concentrations. The data were first analyzed individually by nonlinear, least-squares (NLLS) methods using a single-ideal species model [$n = 1$ in eq 1 (Materials and Methods)] to estimate the weight-average buoyant molecular mass [$\bar{M}_b = \bar{M} (1 - \bar{v}\rho)$]. At each loading concentration, the resulting \bar{M}_b was equal to that expected for a MutL dimer (Figure 3). Similar results were obtained for MutL dialyzed against buffer M with 1 mM MgCl₂ in the presence of 35 μM AMPPNP (data not shown). All of the data were then fit globally by NLLS methods, using a single-ideal species model [$n = 1$ in eq 1 (Materials and Methods)] and assuming a partial specific volume ($\bar{v}_{5^\circ\text{C}}$) of 0.7329 mL/g for MutL (estimated from the amino acid composition of MutL(47) and eq 2). Representative data sets obtained in buffer M (1.9, 0.95, and 0.475 μM monomer) and buffer M with 35 μM AMPPNP and 1 mM MgCl₂ (2.77, 1.38, and 0.69 μM monomer) are shown in panels A and B of Figure 4, respectively. For apo MutL, the calculated molar mass ($M = 130.5 \pm 3.0$ kDa) is only ~4% lower than that expected for the MutL dimer ($M_{\text{MutL}_2} = 135.8$ kDa). Similar results were obtained in buffer M with 1 mM MgCl₂ and 35 μM AMPPNP, with a calculated molar mass of 131.9 ± 4.2 kDa (predicted $M_{\text{MutL}_2\text{-AMPPNP}} = 136.8$ kDa). These results are consistent with MutL being a stable dimer with an extended shape, which becomes more compact upon binding a nonhydrolyzable ATP analogue.

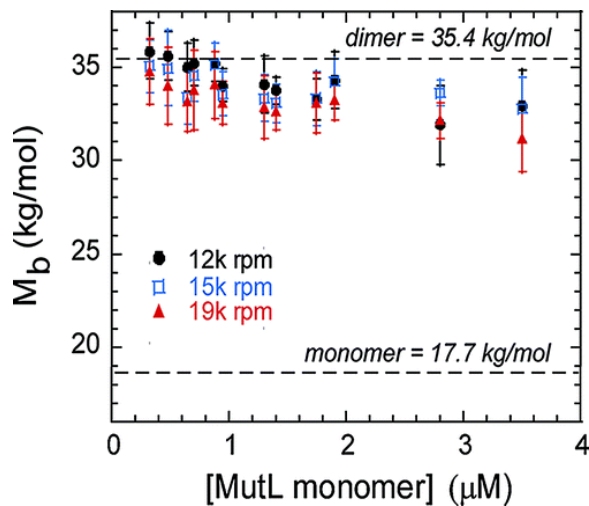


Figure 3. Weight-average buoyant molecular mass, \bar{M}_b , of MutL as a function of protein concentration. M_b was determined with sedimentation equilibrium experiments performed at 5 °C at three rotor speeds (12000, 15000, and 19000 rpm) in buffer M [50 mM potassium phosphate (pH 7.4 at 25 °C), 50 mM KCl, 0.1 mM EDTA, and 1 mM 2-mercaptoethanol]. Each protein concentration distribution was fitted to a single-ideal species model [$n = 1$ in eq 1 (Materials and Methods)]. Values of M_b expected for the MutL monomer and dimer are indicated by dotted lines and calculated assuming monomer $M = 67923.95$ g/mol and $\bar{v}_5^\circ = 0.7329$ mL/g, based on the amino acid sequence of MutL.

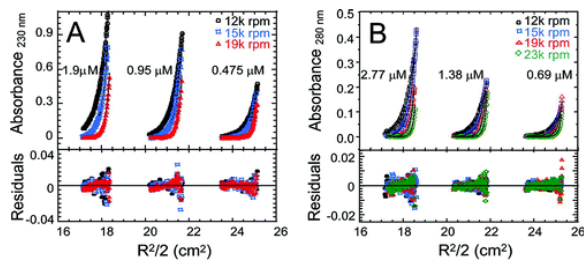


Figure 4. Sedimentation equilibrium data indicate that MutL is a stable dimer. Experiments were performed for three different MutL concentrations indicated on the plot (total monomer loading concentration) at three or four rotor speeds (12000, 15000, 19000, and 23000 rpm) at 5 °C in buffer M (A) or buffer M with 1 mM $MgCl_2$ and 35 μM AMPPNP (B). The smooth curves overlying the data are simulations using the best fit parameters resulting from a global NLLS fit of all data sets to a single-species model with residuals shown below the plots.

Unfortunately, in buffer M, UvrD forms large complexes that cannot be studied easily in the centrifuge. The distribution of UvrD assembly states is sensitive to NaCl and glycerol concentrations.^(28, 60) However, we have been able to determine a set of conditions in which the assembly states of both UvrD and MutL can be studied that supports helicase activity [buffer M20/20 (Table 1)]. Sedimentation equilibrium experiments with MutL were therefore repeated in buffer M20/20 at 25 °C, at four rotor speeds (12000, 15000, 19000, and 23000 rpm) and three MutL concentrations (2.64, 1.32, and 0.66 μM monomer loading concentrations) (Figure 5A). These data were fit globally to a single-ideal species model (Materials and Methods) returning an M of 120.0 ± 5.7 kDa, which is ~ 9 – 11% lower than that expected for a MutL dimer (Figure 5A). Models taking into account hydrodynamic nonideality or monomer–dimer self-association equilibrium did not improve the quality of the fit, and parameters were not constrained (not shown). However, we noticed that \bar{M}_b deviated to a larger extent at higher rotor speeds (longer centrifugation time) and higher MutL concentrations. This observation prompted us to repeat the NLLS fitting for concentration profiles obtained at the two lowest rotor speeds, which yielded an M of 130.2 ± 6.9 kDa, which is the value expected for the MutL dimer. This result suggests that there is some

MutL heterogeneity in buffer M20/20. To further test this idea, we conducted sedimentation velocity studies in buffer M20/20.(50, 61) The $c(s)$ distribution calculated for MutL in buffer M20/20 at 25 °C exhibited one main peak with a symmetrical shape at an $s_{20,w}$ of 4.75 ± 0.02 S (Figure 5B), although an additional minor species ($\sim 4\%$) with a broad peak at an $s_{20,w}$ of $\approx 7.6 \pm 0.2$ S was also present. The $\bar{s}_{20,w}$, calculated by integration of $c(s)$ over both peaks, increases slightly with increasing MutL concentrations with an average value of 4.88 ± 0.04 S (Figure 5C), yielding an f/f_0 of 1.69 ± 0.01 . We conclude that in buffer M20/20 at 25 °C MutL is an elongated dimer, accompanied by a minor population (4%) of larger aggregates that are not in equilibrium with the dimeric form under the conditions and over the time intervals used in our experiments.

Figure 5

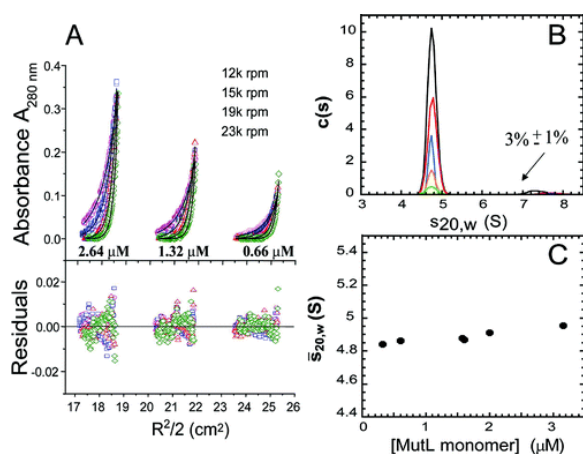


Figure 5. MutL is a dimer in buffer M20/20. (A) Sedimentation equilibrium experiments were performed for three MutL concentrations (2.64, 1.32, and 0.66 μM monomer) at four rotor speeds (12000, 15000, 19000, and 23000 rpm) at 25 °C in buffer M20/20. The smooth curves overlying the absorbance data collected at a wavelength of 280 nm are simulations using the best fit parameters resulting from the global NLLS fit of all data sets to a single-species model with residuals shown below the plot. (B) $c(s)$ distribution for MutL (3.16, 2, 1.6, 0.6, and 0.32 μM monomer) in buffer M20/20 at 25 °C. The absorbance scans were analyzed using SEDFIT. (C) Weight-average sedimentation coefficient, $\bar{s}_{20,w}$, as a function of MutL concentration (micromolar monomer). Values of $\bar{s}_{20,w}$ were obtained by integration of $c(s)$ curves.

Assembly State of MutL Bound to DNA

Recent genetic and biochemical data strongly suggest that DNA binding by MutL is required for MMR *in vivo*.(6, 62) Furthermore, MutL has been shown to stimulate the helicase activity of UvrD.(22, 26, 62) DNA binding of MutL has been investigated previously using an electrophoretic mobility shift assay, nitrocellulose filter binding, and surface plasmon resonance and by following the stimulation of the ATPase activity of MutL in the presence of a DNA cofactor.(7, 9, 25, 26, 38, 62-64) Here we investigated the DNA binding properties of MutL on the DNA substrate that we have used previously to study the helicase activity of UvrD(20, 29, 30, 34) using sedimentation velocity and equilibrium techniques. The DNA consisted of an 18 bp duplex possessing a 3'-dT₂₀ tail with a Cy3 chromophore attached covalently to the blunt DNA end via the 5'-end [3'(dT₂₀)-ds18-Cy3]. Using the Cy3 label as a reporter, one can monitor the sedimentation profile of the DNA via the absorbance of the Cy3 chromophore (at 550 nm) without interference from MutL. Experiments were performed at different ratios of MutL dimer to DNA in buffer M20/20 at 25 °C (Figure 6).

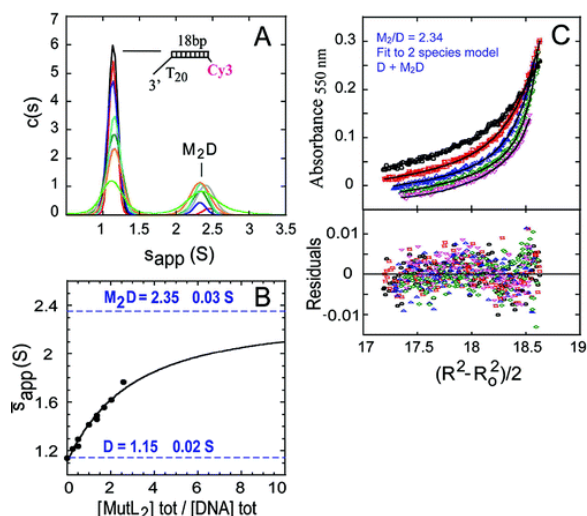


Figure 6. Sedimentation velocity (A and B) and sedimentation equilibrium (C) study of the binding of MutL dimer (M_2) to a Cy3-labeled DNA unwinding substrate [a 3'-(dT₂₀)-ds18 DNA with a Cy3 fluorophore attached to the 5'-end of the bottom strand of the duplex, depicted schematically]. Experiments were performed in buffer M20/20 at 25 °C using a total loading Cy3-DNA concentration of 1.38 (A) or 1.2 μ M (C). The absorbance profiles of Cy3 were monitored at 550 nm. (A) Sedimentation velocity experiments were performed at 42000 rpm. Continuous sedimentation coefficient distribution $c(s)$ of Cy3-DNA in the presence of increasing MutL dimer concentrations (loading molar ratios of MutL dimer to DNA of 0, 0.25, 0.5, 1, 1.37, 2, and 2.59). Sedimentation coefficients are apparent, without correction to the standard conditions. Weight-average sedimentation coefficients obtained by integration of area under the $c(s)$ are depicted in panel B as a function of the MutL dimer:DNA concentration ratio. The smooth curve is a simulation using the best fit parameters derived from NLLS analysis of the data to a simple Langmuir isotherm [apparent binding constant of $(34 \pm 4.3) \times 10^4 \text{ M}^{-1}$ (eq 6 in Materials and Methods)]. (C) Cy3 absorbance profile for a representative sedimentation equilibrium experiment conducted in a 2.34-fold molar excess of MutL dimer over Cy3-DNA at 12000, 15000, 18000, 22000, and 27000 rpm. Data were analyzed by NLLS analysis using a model that assumed the presence of two sedimenting species in solution, one corresponding to the free Cy3-DNA and the other corresponding to DNA bound in complex with MutL dimer [$n = 2$ in eq 1 (Materials and Methods)]. The buoyant molecular mass of the free Cy3-DNA was fixed at a value of $6.66 \pm 0.22 \text{ kg/mol}$, which was obtained experimentally under the same conditions. A best fit value of buoyant molecular mass of the MutL–DNA complex equal to $39.605 \pm 0.460 \text{ kg/mol}$ was obtained from NLLS analysis, which is in reasonable agreement with a theoretical buoyant molecular mass of a single MutL dimer bound to a Cy3-DNA molecule (35.56 kg/mol). Smooth curves overlaying the data are simulations using best fit parameters with residuals shown below the plots.

The resulting uncorrected $c(s)$ distributions(50, 65) show two well-resolved, symmetrical peaks at 1.15 ± 0.02 and $2.35 \pm 0.03 \text{ S}$ (Figure 6A). The position of the second peak did not change with increasing MutL concentration, suggesting that they represent distinct MutL–DNA species.(66, 67) The first peak at $1.15 \pm 0.02 \text{ S}$ represents free DNA (black curve, Figure 6A). The second peak near 2.35 S represents MutL–DNA complexes. An apparent binding isotherm was constructed by plotting the weight-average sedimentation coefficient as a function of the molar ratio of the MutL dimer to DNA (Figure 6B).(52, 68) This binding isotherm was analyzed assuming that a single MutL dimer binds to each DNA substrate (see below), yielding an apparent binding constant of $(34 \pm 4.3) \times 10^4 \text{ M}^{-1}$ (eq 6 in Materials and Methods). The smooth curve in Figure 6B is a simulation using the best fit parameters derived from the NLLS fit of the data to a 1:1 binding isotherm. These data suggest that MutL has a low affinity for DNA and does not bind stoichiometrically under our experimental conditions (i.e., not all added MutL forms a complex with the DNA).

To determine the molecular mass of the MutL–DNA complex corresponding to the 2.35 S species, we performed a sedimentation equilibrium experiment. Figure 6C shows a representative set of concentration profiles collected in buffer M20/20 at 25 °C at five different rotor speeds for a 2.34-fold molar excess of MutL dimer over 3′(dT₂₀)-ds18-Cy3. These absorbance profiles were analyzed using a two-species model, one corresponding to the free Cy3-labeled DNA and the other to a MutL–DNA complex. The buoyant molecular mass (M_b) of the Cy3-DNA molecule was fixed at 6.66 ± 0.22 kg/mol based on independent sedimentation equilibrium experiments performed with free DNA (Materials and Methods). From NLLS analysis of the data in Figure 6C, we obtain a best fit M_b value of 39.61 ± 0.46 kg/mol for the MutL–DNA complex. This value is only slightly higher than the buoyant molecular mass expected for a single MutL dimer bound to the Cy3-DNA molecule (M_{2D}) [$M_{b,M_2D} = 35.56$ kg/mol (Materials and Methods)]. When the experiment was repeated at a 1.25-fold molar excess of the MutL dimer over DNA, we obtained an M_b of 39.16 ± 0.76 kg/mol, similar to the value obtained at higher molar ratios. Including an additional species in the NLLS analysis did not improve the quality of the fit and resulted in unconstrained fitting parameters (data not shown). Thus, over the concentration range studied, these results indicate that a single MutL dimer binds to a 3′(dT₂₀)-ds18 DNA.

On the basis of the stoichiometry of the MutL–DNA complex (M_2D), we calculated a weight-average partial specific volume, \bar{v}_{MutL_2-DNA} , of 0.7237 mL/g at 25 °C (eq 2 in Materials and Methods) for a single MutL dimer bound to the DNA. This can be used to correct the value of the apparent sedimentation coefficient of the M_2D complex to standard conditions [$s_{20,w}$ (see Materials and Methods)] and to obtain an estimate of the frictional coefficient ratio for the M_2D complex (eq 4 in Materials and Methods). For the MutL dimer bound to the 3′(dT₂₀)-ds18-Cy3 DNA, we obtain an $s_{20,w}$ of 5.00 ± 0.06 S and an fff_0 of 1.90 ± 0.02 , which suggests that the M_2D complex is quite asymmetric.

MutL–DNA Complexes in the Presence of AMPPNP

It was reported previously that MutL displays enhanced DNA binding activity in the presence of AMPPNP.(6, 26, 38, 62) An apparent binding constant of 4×10^7 M⁻¹ was measured for MutL binding to DNA (93-nucleotide primer annealed to M13 ssDNA) in 25 mM Tris (pH 7.5 at 22 °C), 20 mM NaCl, 3 mM MgCl₂, 5 mM 2-mercaptoethanol, and 50 µg/mL BSA, whereas a 10-fold higher binding constant of 36×10^7 M⁻¹ was measured in the presence of 3 mM AMPPNP.(26, 62) Moreover, it was suggested that an ATP-bound form of MutL continuously loads UvrD onto a DNA substrate.(6, 21) In light of these results, and considering the AMPPNP-induced conformational change in MutL (see above), it was of interest to study the hydrodynamic properties and stoichiometry of the ternary MutL–AMPPNP–DNA complex. Sedimentation velocity experiments were performed at different ratios of MutL to 3′(dT₂₀)-ds18-Cy3 DNA in the presence or absence of 0.4 mM AMPPNP in buffer M20/20 at 25 °C (Figure 7).

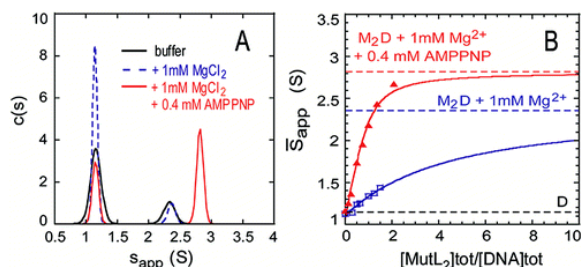


Figure 7. Sedimentation velocity study of binding of MutL dimer to a 3′(dT₂₀)-ds18 DNA. Experiments were performed at 25 °C using a total loading Cy3-DNA concentration of 1.4 µM as a function of MutL dimer concentration in M20/20 (buffer), with 1 mM MgCl₂ (+1 mM MgCl₂), or in M20/20 with 1 mM MgCl₂ and 0.4 mM AMPPNP (+1 mM MgCl₂+0.4 mM AMPPNP). The DNA concentration profiles were recorded by monitoring the absorbance of Cy3 at 550 nm. (A) Sedimentation velocity experiments were performed at 42000 rpm. Representative $c(s)$ distribution of Cy3-DNA in the presence of 1.4 µM MutL dimer ($M_2:D$ molar ratio of 1).

Sedimentation coefficients are not corrected to the standard conditions. (B) Weight-average sedimentation coefficient as a function of the molar ratio of MutL dimer to DNA. The smooth curves are simulations using the best fit parameters derived from NLLS analysis of the data to a simple Langmuir isotherm and assuming that the plateau corresponds to the apparent s value for the MutL–DNA complex [+MgCl₂, 2.36 ± 0.02 S, apparent binding constant of $(19 \pm 1.8) \times 10^4$ M⁻¹; +MgCl₂+AMPPNP, 2.82 ± 0.02 S, apparent binding constant of $(38 \pm 2.5) \times 10^5$ M⁻¹ (eq 6 in Materials and Methods)].

A representative data set obtained at a ratio of 1 MutL dimer per DNA is shown in Figure 7A. Plotting the \bar{s}_{app} as a function of MutL concentration in the presence or absence of 0.4 mM AMPPNP shows that AMPPNP enhances the affinity of MutL for 3'(dT₂₀)-ds18-Cy3 DNA (Figure 7B) and yields an apparent binding constant of $(38 \pm 2.5) \times 10^5$ M⁻¹ (eq 6 in Materials and Methods). In the absence of AMPPNP, binding of MutL to DNA is 20-fold weaker with an apparent binding constant of $(1.96 \pm 0.2) \times 10^5$ M⁻¹ (Figure 7B). These results show that the increased level of M₂D complex formation is due to AMPPNP binding to MutL. MutL, in the presence of both Mg²⁺ and AMPPNP, forms a stable, well-defined protein–DNA species, because the position of the peak reflecting the MutL–DNA complex does not change with increasing protein concentrations (data not shown). Analogous behavior was also observed in buffer M20/20 (Figure 6A), which suggests that the MutL–DNA equilibrium dynamics are slow in comparison to the time scale of sedimentation velocity.(52, 66, 67) In the presence of 1 mM MgCl₂ in buffer M20/20, for all MutL concentrations studied the $c(s)$ distributions show two well-resolved and symmetrical peaks centered at 1.14 ± 0.02 and 2.36 ± 0.02 S (Figure 7A), consistent with what was observed in buffer M20/20 (Figure 6A), suggesting that a single MutL dimer binds per 3'(dT₂₀)-ds18-Cy3 DNA. The values of the sedimentation coefficients corrected to standard conditions are as follows: $s_{20,w} = 2.23 \pm 0.02$ S for DNA, and $s_{20,w} = 5.02 \pm 0.05$ S for the M₂D complex (similar to the values in buffer M20/20, suggesting a similar hydrodynamic shape for both macromolecular species).

In the presence of 1 mM MgCl₂ and 0.4 mM AMPPNP (buffer M20/20), the two well-resolved and symmetrical $c(s)$ peaks are centered at 1.16 ± 0.01 and 2.82 ± 0.02 S (Figure 7A and data not shown), which upon correction to standard conditions yields $s_{20,w}$ values of 2.25 ± 0.03 S for DNA and 5.99 ± 0.05 S for the MutL–DNA–AMPPNP ternary complex (M₂D–AMPPNP). The $s_{20,w}$ for the M₂D–AMPPNP complex is higher than that of the M₂D complex in the presence and absence of Mg²⁺. The calculated frictional coefficient ratio (eq 4 in Materials and Methods) for the ternary complex is 1.61 ± 0.01 , which is lower than the value in the absence of nucleotide [1.90 ± 0.02 (see above)], suggesting that the M₂D complex becomes more compact upon AMPPNP binding.(24, 38) Sedimentation velocity experiments performed at a 1:1 molar ratio of MutL dimer to Cy3-DNA (buffer M20/20 with 1 mM MgCl₂), as a function of AMPPNP concentration (Figure 1 of the Supporting Information), show that the concentration of the nucleotide cofactor used in our studies (400 μM) is saturating. Data in Figure 1 of the Supporting Information were analyzed using a model that assumes two identical and independent AMPPNP binding sites per MutL dimer (eq 5 in Materials and Methods), returning an apparent binding constant of $(7.0 \pm 2.8) \times 10^4$ M⁻¹.

Discussion

Knowledge of the assembly state of any enzyme is needed to fully understand the molecular mechanism of its function and to facilitate interpretation of the thermodynamics of its interactions with its substrates and cofactors. In previous studies, a range of assembly states of full-length MutL has been observed using a variety of approaches, including glycerol gradient centrifugation, gel filtration chromatography, and dynamic light scattering techniques.(7, 39) In 50 mM potassium phosphate (pH 7.4), 50 mM KCl, 0.1 mM EDTA, and 1 mM DTT at 3 °C, MutL was found to have an $s_{20,w}$ of 5.5 S and a Stokes radius of 61 Å, suggesting a dimer with an asymmetric shape ($f/f_0 = 1.8$). (39) Dynamic light scattering experiments performed at 24 °C in 20 mM Tris (pH 8.0), 200 mM KCl, 5 mM MgCl₂, 1 mM DTT, and 0.1 mM EDTA suggested that MutL has a Stokes radius of 86 Å

that decreases to 56 Å upon binding of AMPPNP.(7) The dimensions of the MutL dimer calculated from these two studies differ substantially. This difference could result from differences in protein concentration or solution conditions (i.e., buffer composition and/or temperature) used in the two studies. Changes in any of these parameters can potentially influence the MutL assembly state as we have shown here.

MutL Can Self-Associate To Form Higher-Order Oligomeric Species

Our sedimentation velocity analysis of MutL shows that solutions without phosphate promote MutL to self-associate into larger heterogeneous oligomeric species. The extent of MutL heterogeneity and the average size of the species formed were both reduced at lower temperatures, lower protein concentrations, and higher NaCl concentrations. Ban and Yang(24) noted previously that full-length MutL “tends to aggregate”, although this self-association process was not studied further.

The structure of the MutL C-terminal 20 kDa domain shows a dimer, whereas the N-terminal domain is monomeric in the absence of nucleotide but forms a dimer when bound to AMPPNP.(24, 38) A model based on the crystal structures proposes that MutL forms a stable dimer through its C-terminal domains connected to their respective N-terminal domains by unstructured linkers that undergo ATP-dependent conformational changes leading to communication with MutS and MthH during mismatch repair.(7) The propensity of MutL to self-associate beyond a dimer may be due to the partially unfolded and “monomeric” state of the N-terminal domain.(38) The observation that the MutL–AMPPNP complex forms more stable dimers in solution(24) supports this idea. Interestingly, in buffer M (Table 1) for monomer loading concentrations of 0.2–5 μM, we detect only dimers of MutL (Figures 2 and 3). Furthermore, MutL remains dimeric over a similar concentration range in buffer M containing 10 mM to 1 M KCl or in the presence of 20% (v/v) glycerol, suggesting that a dimer is a stable oligomeric state of MutL. Buffer M was used previously by Modrich and co-workers for purification, storage, and preliminary characterization of MutL,(39) and our results are consistent with their studies of the MutL assembly state under these conditions.

The dimeric state of MutL observed in buffer M is in sharp contrast to the highly heterogeneous distribution of multimeric species observed in Tris buffers. Our sedimentation velocity experiments suggest that the presence of phosphate at pH 7.4 stabilizes the MutL dimer relative to these higher-order aggregates. Because MutL is an ATPase, it is possible that PO_4^{3-} , which is one of the products of ATP hydrolysis, binds to the ATP binding pocket and stabilizes the disordered surfaces in apo MutL, such that the protein is no longer prone to further self-association beyond a dimer. Even if this is the case, the N-termini of MutL do not fully fold and/or dimerize in buffer containing potassium phosphate as it is observed only upon AMPPNP binding.

Monovalent cations such as sodium and potassium may also contribute to MutL stability by stabilizing the conformation of the ATP pocket lid. In addition to magnesium, which is essential for catalysis, a potassium ion is observed to be bound adjacent to the triphosphate moiety of ADPNP in the crystal structure of the N-terminal 40 kDa fragment of MutL.(69) The potassium ion is coordinated by four carbonyl oxygen atoms that originate from amino acids located at the N-terminal hinge of the ATP lid, and a water molecule, such that the monovalent cation may stabilize the ATP pocket lid.(69)

Hydrodynamic Properties of MutL Dimers

We performed both sedimentation velocity and equilibrium experiments over a wide range of MutL concentrations (0.25–5 μM monomer), under identical solution conditions in the absence and presence of the nonhydrolyzable ATP analogue, AMPPNP. Analysis of the sedimentation equilibrium data unequivocally shows that apo and AMPPNP-bound MutL are dimeric in buffer M (5 and 25 °C). From the sedimentation coefficient of MutL ($\bar{s}_{20,w} = 5.20 \pm 0.08$ S for nucleotide free and $\bar{s}_{20,w} = 5.71 \pm 0.08$ S for AMPPNP-bound MutL dimer), we can calculate the f/f_0 ratio (eq 4 in Materials and Methods),(28, 53, 54) which reflects the overall shape of the protein.(52, 70) For apo and AMPPNP-bound MutL, these differ substantially with f/f_0 values of 1.58 ± 0.02 and

1.45 ± 0.02, respectively. These values indicate that both dimers are highly extended and/or possess disordered and/or unfolded regions.(53, 70, 71) However, when AMPPNP binds, the overall shape of the MutL dimer changes. In light of the available crystal structures of the N-terminal fragment of MutL, we suggest that this reflects the folding and dimerization of the partially disordered monomeric N-termini of the MutL dimer, resulting in a more compact structure. Similar hydrodynamic parameters for the MutL dimer were obtained in buffer M20/20 ($\bar{s}_{20,w} = 4.88 \pm 0.04$ S, and $f/f_0 = 1.69 \pm 0.01$). Our results are in good agreement with values reported by Modrich and co-workers.(39) The differences between those results and other studies(7) are likely due to the lack of phosphate in the latter experiments, conditions that we have shown here to facilitate further aggregation of MutL beyond a dimer.

Stoichiometry and Hydrodynamic Properties of a MutL–DNA Complex

We also examined the stoichiometry of MutL bound to 3'(dT₂₀)-ds18 DNA in buffer M20/20 with or without 1 mM MgCl₂ as well as in the presence of 1 mM MgCl₂ and 0.4 mM AMPPNP. With a 2.5-fold molar excess of MutL dimer over DNA, we detect a single species composed of one MutL dimer bound to one DNA molecule. In the presence of 1 mM MgCl₂, $s_{20,w} = 5.02 \pm 0.05$ S for the M₂D complex, yielding an f/f_0 of 1.90 ± 0.02 (similar values were obtained without MgCl₂). In the presence of 1 mM MgCl₂ and 0.4 mM AMPPNP, a distinct ternary complex is formed with an $s_{20,w}$ of 5.99 ± 0.05 S, yielding an f/f_0 of 1.61 ± 0.01 . Our results suggest that upon binding AMPPNP, the highly asymmetrical M₂D complex becomes more compact, likely because of the folding and dimerization of the N-termini of MutL and concomitant closure of the central channel possibly encircling the DNA. This conformational change has not previously been observed, although it was postulated on the basis of molecular modeling of full-length MutL.(7, 38)

Although in buffer M20/20 MutL binds weakly to 3'(dT₂₀)-ds18 DNA [apparent binding constant of $(34 \pm 4.3) \times 10^4$ M⁻¹], and the presence of 1 mM MgCl₂ further weakens the interaction (~2-fold), in the presence of 0.4 mM AMPPNP and 1 mM MgCl₂, the level of binding increases by 1 order of magnitude [apparent binding constant of $(38 \pm 2.5) \times 10^5$ M⁻¹]. In the crystal structure of the dimeric N-terminal MutL fragment bound to AMPPNP, a deep, saddle-shaped groove with high positive electrostatic surface potential is formed between two subunits that can accommodate ssDNA.(38) It was proposed that this saddle constitutes a DNA binding site, and this proposal is supported by mutational analysis.(6, 25, 38, 62) Previous filter binding studies performed in 25 mM Tris (pH 7.5), 100 mM NaCl, 3 mM MgCl₂, 5 mM 2-mercaptoethanol, and 3 mM AMPPNP at 37 °C estimated a binding constant of 24×10^4 M⁻¹ for MutL binding to a 50 bp duplex with a 20-nucleotide 3'-overhang.(62) In our studies, we have measured an apparent binding constant of $(38 \pm 2.5) \times 10^5$ M⁻¹ for MutL binding to an 18 bp duplex with a 3'-(dT)₂₀ tail (Cy3-labeled). These differences likely reflect differences in solution conditions, DNA, and the methods employed for measuring affinity.

Recently, a computational analysis of all protein interfaces observed in the crystal structure of the C-terminal domain of MutL was reported.(72) On the basis of this, it was suggested that the biologically relevant dimer interface is different from that proposed in the original report,(7) leading to a revised model of full-length MutL(72) that seems compatible with the results of cross-linking experiments. Deletion of the 10 C-terminal amino acid residues of MutL, which form part of the interface in the revised dimer, inhibits dimer formation based on gel filtration experiments.(72) In another study, a dimeric structure for a similar deletion was observed in both gel filtration and analytical ultracentrifugation experiments,(21) which would suggest that the originally proposed interface is correct. The origin of this discrepancy is not clear, although it may be that the high salt concentration (500 mM NaCl and separation of MutL oligomeric species via size exclusion chromatography) used in the former study(72) may facilitate dimer disruption. Our data show that MutL has an elongated hydrodynamic shape that in principle agrees with both models. Mutagenic analysis of these predicted dimerization interfaces is required to further probe the oligomeric nature of MutL.

Supporting Information

Figure 1, Table 1 summarizing all the sedimentation coefficients measured in this study, and Table 2 summarizing all the binding constants for AMPPNP and DNA binding to MutL. This material is available free of charge via the Internet at <http://pubs.acs.org>.

Terms & Conditions

Most electronic Supporting Information files are available without a subscription to ACS Web Editions. Such files may be downloaded by article for research use (if there is a public use license linked to the relevant article, that license may permit other uses). Permission may be obtained from ACS for other uses through requests via the RightsLink permission system: <http://pubs.acs.org/page/copyright/permissions.html>.

Acknowledgment

We thank Paul Modrich (Duke University, Durham, NC) for providing the MutL overexpression plasmid and Thang Ho for synthesis and purification of oligodeoxynucleotides.

Abbreviations

MMR	methyl-directed mismatch repair
SF1	superfamily 1
NLLS	nonlinear least-squares.

References

- 1 Iyer, R. R., Pluciennik, A., Burdett, V., and Modrich, P. L. (2006) DNA mismatch repair: Functions and mechanisms *Chem. Rev.* 106, 302– 323
- 2 Hsieh, P. (2001) Molecular mechanisms of DNA mismatch repair *Mutat. Res.* 486, 71– 87
- 3 Kunkel, T. A. and Erie, D. A. (2005) DNA mismatch repair *Annu. Rev. Biochem.* 74, 681– 710
- 4 Yang, W. (2000) Structure and function of mismatch repair proteins *Mutat. Res.* 460, 245– 256
- 5 Su, S. S. and Modrich, P. (1986) *Escherichia coli mutS*-encoded protein binds to mismatched DNA base pairs *Proc. Natl. Acad. Sci. U.S.A.* 83, 5057– 5061
- 6 Robertson, A. B., Pattishall, S. R., Gibbons, E. A., and Matson, S. W. (2006) MutL-catalyzed ATP hydrolysis is required at a post-UvrD loading step in methyl-directed mismatch repair *J. Biol. Chem.* 281, 19949– 19959
- 7 Guarne, A., Ramon-Maiques, S., Wolff, E. M., Ghirlando, R., Hu, X., Miller, J. H., and Yang, W. (2004) Structure of the MutL C-terminal domain: A model of intact MutL and its roles in mismatch repair *EMBO J.* 23, 4134– 4145
- 8 Grilley, M., Griffith, J., and Modrich, P. (1993) Bidirectional excision in methyl-directed mismatch repair *J. Biol. Chem.* 268, 11830– 11837
- 9 Acharya, S., Foster, P. L., Brooks, P., and Fishel, R. (2003) The coordinated functions of the *E. coli* MutS and MutL proteins in mismatch repair *Mol. Cell* 12, 233– 246
- 10 Allen, D. J., Makhov, A., Grilley, M., Taylor, J., Thresher, R., Modrich, P., and Griffith, J. D. (1997) MutS mediates heteroduplex loop formation by a translocation mechanism *EMBO J.* 16, 4467– 4476
- 11 Junop, M. S., Obmolova, G., Rausch, K., Hsieh, P., and Yang, W. (2001) Composite active site of an ABC ATPase: MutS uses ATP to verify mismatch recognition and authorize DNA repair *Mol. Cell* 7, 1– 12
- 12 Yang, W., Junop, M. S., Ban, C., Obmolova, G., and Hsieh, P. (2000) DNA mismatch repair: From structure to mechanism *Cold Spring Harbor Symp. Quant. Biol.* 65, 225– 232
- 13 Matson, S. W. (1986) *Escherichia coli* helicase II (uvrD gene product) translocates unidirectionally in a 3' to 5' direction *J. Biol. Chem.* 261, 10169– 10175

- 14 Georgi-Geisberger, P. and Hoffmann-Berling, H. (1990) Direction of the DNA-unwinding reaction catalysed by *Escherichia coli* DNA helicase II Eur. J. Biochem. 192, 689– 693
- 15 Runyon, G. T., Bear, D. G., and Lohman, T. M. (1990) *Escherichia coli* helicase II (UvrD) protein initiates DNA unwinding at nicks and blunt ends Proc. Natl. Acad. Sci. U.S.A. 87, 6383– 6387
- 16 Dao, V. and Modrich, P. (1998) Mismatch-, MutS-, MutL-, and helicase II-dependent unwinding from the single-strand break of an incised heteroduplex J. Biol. Chem. 273, 9202– 9207
- 17 Burdett, V., Baitinger, C., Viswanathan, M., Lovett, S. T., and Modrich, P. (2001) In vivo requirement for RecJ, ExoVII, ExoI, and ExoX in methyl-directed mismatch repair Proc. Natl. Acad. Sci. U.S.A. 98, 6765– 6770
- 18 Viswanathan, M., Burdett, V., Baitinger, C., Modrich, P., and Lovett, S. T. (2001) Redundant exonuclease involvement in *Escherichia coli* methyl-directed mismatch repair J. Biol. Chem. 276, 31053– 31058
- 19 Lahue, R. S., Au, K. G., and Modrich, P. (1989) DNA mismatch correction in a defined system Science 245, 160– 164
- 20 Ali, J. A. and Lohman, T. M. (1997) Kinetic measurement of the step size of DNA unwinding by *Escherichia coli* UvrD helicase Science 275, 377– 380
- 21 Matson, S. W. and Robertson, A. B. (2006) The UvrD helicase and its modulation by the mismatch repair protein MutL Nucleic Acids Res. 34, 4089– 4097
- 22 Yamaguchi, M., Dao, V., and Modrich, P. (1998) MutS and MutL activate DNA helicase II in a mismatch-dependent manner J. Biol. Chem. 273, 9197– 9201
- 23 Hall, M. C., Jordan, J. R., and Matson, S. W. (1998) Evidence for a physical interaction between the *Escherichia coli* methyl-directed mismatch repair proteins MutL and UvrD EMBO J. 17, 1535– 1541
- 24 Ban, C. and Yang, W. (1998) Crystal structure and ATPase activity of MutL: Implications for DNA repair and mutagenesis Cell 95, 541– 552
- 25 Junop, M. S., Yang, W., Funchain, P., Clendenin, W., and Miller, J. H. (2003) In vitro and in vivo studies of MutS, MutL and MutH mutants: Correlation of mismatch repair and DNA recombination DNA Repair 2, 387– 405
- 26 Mechanic, L. E., Frankel, B. A., and Matson, S. W. (2000) *Escherichia coli* MutL loads DNA helicase II onto DNA J. Biol. Chem. 275, 38337– 38346
- 27 Runyon, G. T. and Lohman, T. M. (1993) Kinetics of *Escherichia coli* helicase II-catalyzed unwinding of fully duplex and nicked circular DNA Biochemistry 32, 4128– 4138
- 28 Maluf, N. K. and Lohman, T. M. (2003) Self-association equilibria of *Escherichia coli* UvrD helicase studied by analytical ultracentrifugation J. Mol. Biol. 325, 889– 912
- 29 Maluf, N. K., Fischer, C. J., and Lohman, T. M. (2003) A dimer of *Escherichia coli* UvrD is the active form of the helicase in vitro J. Mol. Biol. 325, 913– 935
- 30 Ali, J. A., Maluf, N. K., and Lohman, T. M. (1999) An oligomeric form of *E. coli* UvrD is required for optimal helicase activity J. Mol. Biol. 293, 815– 834
- 31 Lohman, T. M., Tomko, E. J., and Wu, C. G. (2008) Non-hexameric DNA helicases and translocases: Mechanisms and regulation Nat. Rev. Mol. Cell Biol. 9, 391– 401
- 32 Heller, R. C. and Marians, K. J. (2007) Non-replicative helicases at the replication fork DNA Repair 6, 945– 952
- 33 Sun, B., Wei, K. J., Zhang, B., Zhang, X. H., Dou, S. X., Li, M., and Xi, X. G. (2008) Impediment of *E. coli* UvrD by DNA-destabilizing force reveals a strained-inchworm mechanism of DNA unwinding EMBO J. 27, 3279– 3287
- 34 Fischer, C. J., Maluf, N. K., and Lohman, T. M. (2004) Mechanism of ATP-dependent translocation of *E. coli* UvrD monomers along single-stranded DNA J. Mol. Biol. 344, 1287– 1309
- 35 Tomko, E. J., Fischer, C. J., Niedziela-Majka, A., and Lohman, T. M. (2007) A nonuniform stepping mechanism for *E. coli* UvrD monomer translocation along single-stranded DNA Mol. Cell 26, 335– 347
- 36 Tomko, E. J., Jia, H., Park, J., Maluf, N. K., Ha, T., and Lohman, T. M. (2010) 5'-Single-stranded/duplex DNA junctions are loading sites for *E. coli* UvrD translocase EMBO J. 29, 3826– 3839
- 37 Brendza, K. M., Cheng, W., Fischer, C. J., Chesnik, M. A., Niedziela-Majka, A., and Lohman, T. M. (2005) Autoinhibition of *Escherichia coli* Rep monomer helicase activity by its 2B subdomain Proc. Natl. Acad. Sci. U.S.A. 102, 10076– 10081

- 38 Ban, C., Junop, M., and Yang, W. (1999) Transformation of MutL by ATP binding and hydrolysis: A switch in DNA mismatch repair *Cell* 97, 85– 97
- 39 Grilley, M., Welsh, K. M., Su, S. S., and Modrich, P. (1989) Isolation and characterization of the *Escherichia coli mutL* gene product *J. Biol. Chem.* 264, 1000– 1004
- 40 Fritsch, E. F., Sambrook, J., and Maniatis, T. (1989) *Molecular Cloning: A Laboratory Manual*, Vol. 1, Cold Spring Harbor Laboratory Press, Plainview, NY.
- 41 Lohman, T. M., Chao, K., Green, J. M., Sage, S., and Runyon, G. T. (1989) Large-scale purification and characterization of the *Escherichia coli rep* gene product *J. Biol. Chem.* 264, 10139– 10147
- 42 Wong, I., Chao, K. L., Bujalowski, W., and Lohman, T. M. (1992) DNA-induced dimerization of the *Escherichia coli rep* helicase. Allosteric effects of single-stranded and duplex DNA *J. Biol. Chem.* 267, 7596– 7610
- 43 Kozlov, A. G. and Lohman, T. M. (2002) Stopped-flow studies of the kinetics of single-stranded DNA binding and wrapping around the *Escherichia coli* SSB tetramer *Biochemistry* 41, 6032– 6044
- 44 Holbrook, J. A., Capp, M. W., Saecker, R. M., and Record, M. T., Jr. (1999) Enthalpy and heat capacity changes for formation of an oligomeric DNA duplex: Interpretation in terms of coupled processes of formation and association of single-stranded helices *Biochemistry* 38, 8409– 8422
- 45 Laue, T. M., Shah, B. D., Ridgeway, T. M., and Pelletier, S. L. (1992) *Computer-aided interpretation of analytical sedimentation data for proteins*, Vol. 1, Royal Society of Chemistry, Cambridge, U.K.
- 46 Johnson, M. L., Correia, J. J., Yphantis, D. A., and Halvorson, H. R. (1981) Analysis of data from the analytical ultracentrifuge by nonlinear least-squares techniques *Biophys. J.* 36, 575– 588
- 47 Cohn, E. J. and Edsall, J. T. (1943) *Proteins, Amino Acids and Peptides as Ions and Dipolar Ions*, Vol. 1, Rheinhold, New York.
- 48 Durchschlag, H. (1986) *Specific volumes of biological macromolecules and some other molecules of biological interest*, Vol. 1, Springer-Verlag, New York.
- 49 Schuck, P. (1998) Sedimentation analysis of noninteracting and self-associating solutes using numerical solutions to the Lamm equation *Biophys. J.* 75, 1503– 1512
- 50 Dam, J. and Schuck, P. (2004) Calculating sedimentation coefficient distributions by direct modeling of sedimentation velocity concentration profiles *Methods Enzymol.* 384, 185– 212
- 51 Svedberg, T. (1940) *The Ultracentrifuge*, Johnson Reprint Corp., New York.
- 52 Schuck, P. (2005) *Diffusion-Deconvoluted Sedimentation Coefficient Distributions for the Analysis of Interacting and Non-Interacting Protein Mixtures*, The Royal Society of Chemistry, Cambridge, U.K.
- 53 Cantor, C. R. and Schimmel, P. R. (2002) *Biophysical Chemistry. Part II: Techniques for the Study of Biological Structure and Function*, 12th ed., Vol. II, W. H. Freeman and Co., New York.
- 54 Bujalowski, W., Klonowska, M. M., and Jezewska, M. J. (1994) Oligomeric structure of *Escherichia coli* primary replicative helicase DnaB protein *J. Biol. Chem.* 269, 31350– 31358
- 55 Kuntz, I. D. (1971) Hydration of macromolecules. IV. Polypeptide conformation in frozen solutions *J. Am. Chem. Soc.* 93, 516– 518
- 56 Lin, T. H., Quinn, T., Walsh, M., Grandgenett, D., and Lee, J. C. (1991) Avian myeloblastosis virus reverse transcriptase. Effect of glycerol on its hydrodynamic properties *J. Biol. Chem.* 266, 1635– 1640
- 57 Bastos, M., Castro, V., Mrevlishvili, G., and Teixeira, J. (2004) Hydration of ds-DNA and ss-DNA by neutron quasielastic scattering *Biophys. J.* 86, 3822– 3827
- 58 Kuntz, I. D., Jr. and Kauzmann, W. (1974) Hydration of proteins and polypeptides *Adv. Protein Chem.* 28, 239– 345
- 59 Maluf, N. K., Ali, J. A., and Lohman, T. M. (2003) Kinetic mechanism for formation of the active, dimeric UvrD helicase-DNA complex *J. Biol. Chem.* 278, 31930– 31940
- 60 Runyon, G. T., Wong, I., and Lohman, T. M. (1993) Overexpression, purification, DNA binding, and dimerization of the *Escherichia coli uvrD* gene product (helicase II) *Biochemistry* 32, 602– 612
- 61 Laue, T. (2001) Biophysical studies by ultracentrifugation *Curr. Opin. Struct. Biol.* 11, 579– 583
- 62 Robertson, A., Pattishall, S. R., and Matson, S. W. (2006) The DNA binding activity of MutL is required for methyl-directed mismatch repair in *Escherichia coli* *J. Biol. Chem.* 281, 8399– 8408

- 63** Bende, S. M. and Grafstrom, R. H. (1991) The DNA binding properties of the MutL protein isolated from *Escherichia coli* Nucleic Acids Res. 19, 1549– 1555
- 64** Selmane, T., Schofield, M. J., Nayak, S., Du, C., and Hsieh, P. (2003) Formation of a DNA mismatch repair complex mediated by ATP J. Mol. Biol. 334, 949– 965
- 65** Schuck, P. (2000) Size-distribution analysis of macromolecules by sedimentation velocity ultracentrifugation and Lamm equation modeling Biophys. J. 78, 1606– 1619
- 66** Dam, J. and Schuck, P. (2005) Sedimentation velocity analysis of heterogeneous protein-protein interactions: Sedimentation coefficient distributions $c(s)$ and asymptotic boundary profiles from Gilbert-Jenkins theory Biophys. J. 89, 651– 666
- 67** Dam, J., Velikovsky, C. A., Mariuzza, R. A., Urbanke, C., and Schuck, P. (2005) Sedimentation velocity analysis of heterogeneous protein-protein interactions: Lamm equation modeling and sedimentation coefficient distributions $c(s)$ Biophys. J. 89, 619– 634
- 68** Correia, J. J. (2000) Analysis of weight average sedimentation velocity data Methods Enzymol. 321, 81– 100
- 69** Hu, X., Machius, M., and Yang, W. (2003) Monovalent cation dependence and preference of GHKL ATPases and kinases FEBS Lett. 544, 268– 273
- 70** Tanford, C. (1961) Physical Chemistry of Macromolecules, Wiley, New York.
- 71** Teller, D. C., Swanson, E., and de Haen, C. (1979) The translational friction coefficient of proteins Methods Enzymol. 61, 103– 124
- 72** Kosinski, J., Steindorf, I., Bujnicki, J. M., Giron-Monzon, L., and Friedhoff, P. (2005) Analysis of the quaternary structure of the MutL C-terminal domain J. Mol. Biol. 351, 895– 909